

Magnon Blockade with Skyrmion Qubit-Magnon Coupling in a Hybrid Quantum System

Si-Tong Jin¹,[✉] Shi-wen He,¹ Zi-long Yang,¹ Xuanxuan Xin,² and Chong Li^{1,*}

¹*School of Physics, Dalian University of Technology, Dalian 116024, China*

²*College of Arts and Science, Qingdao Binhai University, Qingdao 266555, China.*

(Dated: December 17, 2024)

Magnon blockade (MB) serves as an efficient mechanism for generating a single magnon, which holds significance in quantum information processing. In this work, we propose a scheme to realize magnon blockade effects in a hybrid system consisting of a YIG micromagnet and a skyrmion. Through numerical simulations, we explore the behavior of the second-order correlation function $g^{(2)}(0)$ under various parameter regimes and examine the influence of the ambient thermal noise on the magnon blockade effects. The results indicate that the behavior of the second-order correlation function for the magnon mode critically depends on the skyrmion qubit-magnon coupling strength and the drive detuning. By tuning the drive field, the system effectively suppresses multi-magnon state and yields a high-purity single-magnon state, exhibiting pronounced antibunching and magnon blockade effects. This scheme provides a feasible and versatile new all-magnetic platform for achieving high-purity single-magnon sources.

I. INTRODUCTION

Hybrid quantum systems leverage the advantages of different quantum subsystems and play a significant role in fields such as quantum information processing, quantum networking, and quantum sensing [1–4]. With high spin density, broad frequency tunability, long lifetime, and enhanced coherence times, magnons excited within YIG materials have emerged as promising candidates for quantum information carriers [5–14]. The unique properties of magnons have facilitated the development of various hybrid magnonic systems, including cavity optomagnonic systems [15–17], cavity magnonic systems [18] and qubit-magnon systems [19–21]. In these platforms, magnon modes can couple effectively with quantum information carriers such as phonon modes, microwave photons, optical photons, and superconducting qubits [22–30]. A variety of nontrivial quantum phenomena have been observed within these configurations, underscoring the potential of hybrid magnonic systems as powerful platforms for probing and controlling complex quantum interactions [25, 29–57]. Recently, coupled skyrmion qubit - magnon systems have emerged as a compelling area of research [58, 59].

Skyrmions, as magnetic nanostructures with particle-like characteristics, display emerging magnetic effects [60–63]. Their most notable attribute is their topological protection [64, 65], which enables skyrmions to withstand external disturbances. This topological protection allows for state manipulation with ultra-low currents, along with the modulation of electric and magnetic fields [58, 66–68], facilitating logical transitions within a richly anharmonic operational regime and making them robust information carriers [60, 69]. Consequently, skyrmions hold significant promise for applications in spintronics and quantum computing [70–80]. Experimentally, skyrmions can be generated in centrosymmetric crystals, such as Gd_2PdSi_3 [81]. In frustrated magnets, skyrmions exhibit internal degrees of freedom related to helicity [81–86]. By quantizing collective helicity coordinates,

two types of qubits can be constructed [66], and with coherence times on the order of microseconds, skyrmion qubits are well-suited for quantum state manipulation. Furthermore, nonvolatile readout methodologies provide a robust means for reliable qubit state measurement. In magnon-skyrmion qubit systems, tunable coherent and dissipative coupling between magnon modes in a YIG micromagnet and the quantized helicity degree of freedom of skyrmions has been achieved [58]. This robust all-magnetic coupling mechanism acts as a mediator to enable long-range coherent interactions with skyrmions, thereby realizing the scalability of skyrmion qubits and providing a promising all-magnetic alternative platform for exploring quantum effects.

In recent years, magnon blockade (MB) has attracted special attention as a purely quantum effect [25, 29, 30, 43–50, 56]. The MB effect was first introduced in the context of a hybrid ferromagnet-superconductor quantum system in 2019 [29]. The standard indicator for verifying a stable single-magnon state is $g^{(2)}(0) \rightarrow 0$ [87–89]. Analogous to photon blockade [51–55, 90, 91] and phonon blockade [92, 93], magnon blockade enables the preparation of single-magnon states, offering the possibility of quantum control at the single-magnon level.

In this paper, we aim to generate a stable and high-fidelity single-magnon state by optimizing the MB effect, where a YIG micromagnet are coupled to a resonant skyrmion qubit via strong interaction [58]. The focus of this work is to systematically investigate the steady-state statistical properties of magnons in a skyrmion qubit-magnon coupled system. By numerically solving the quantum master equation for the systems density matrix [29, 94], we analyze the second-order correlation function $g^{(2)}(0)$, which characterizes the magnon excitation statistics. Our results reveal that $g^{(2)}(0)$ can reach the order of 10^{-6} , indicating a strong the MB effect. This effect can be optimized within a specific range of system parameters. Furthermore, we demonstrate that the MB effect is highly sensitive to the coupling strength between the skyrmion qubit and magnon, as well as to the detuning of the drive field. We also discuss in detail the impact of thermal noise from the systems environment on the MB effect. Beyond its fundamental scientific significance, the exploration of the MB effect is

* Email address: lichong@diut.edu.cn

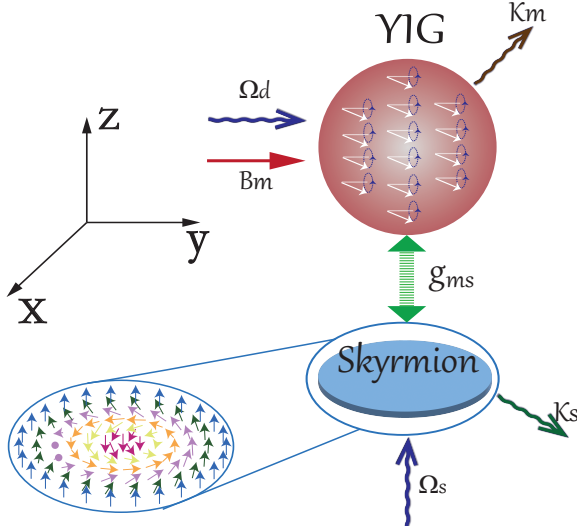


FIG. 1. Schematic representation of the hybrid magnon-Skyrmion system. The magnon is probed by an external microwave field Ω_m , while the skyrmion is driven by a microwave field Ω_s . The magnon mode interacts with the skyrmion mode through a coupling strength g_{ms} . The dissipative processes for both the magnon and skyrmion modes are represented by the damping rates κ_m and κ_s , respectively. Long-lasting spin wave modes are induced by the application of a uniform bias magnetic field B_m . Here, we concentrate on the Kittel mode, characterized by the coherent precession of all spins in the micromagnet, with spins maintaining identical phase and amplitude.

crucial for the study of magnons at the quantum level, and it opens up avenues for designing single-magnon emitters. Thus, Our findings provide a theoretical foundation for achieving single-magnon quantum control within an all-magnetic platform [95].

II. MODEL AND HAMILTONIAN

The physical system considered in our study is a hybrid quantum structure [as illustrated in Fig. 1], which integrates two collective excitation modes: the magnon mode within a ferromagnetic YIG micromagnet and a skyrmion mode positioned beneath it. The strong coupling between them depends on their spatial configuration. Specifically, the vertical distance from the skyrmion to the surface and center of the YIG sphere directly affects the skyrmion qubit-magnon coupling strength, allowing for precise control over the coupling range [58]. Within the YIG sphere, spin wave modes with long coherence times can be induced through the application of a uniform bias magnetic field B_m [58, 96, 97]. The magnon represents spin waves in magnetic materials, which are collective excitations of spin ensembles, while the skyrmion is a topological excitation in magnetic materials, typically manifested as rotations or twists in the spin structure. The coupling between the magnon and the skyrmion can be understood as the interaction between the collective spin wave oscillation of the magnon and the localized spin motion within the skyrmion's

topological structure. The free Hamiltonian associated with the magnon mode can be expressed as $\hat{H}_m = \omega_m \hat{m}^\dagger \hat{m}$ (we set $\hbar = 1$), where \hat{m}^\dagger and \hat{m} represent the creation and annihilation operators of the magnon mode, respectively, and $\omega_m = \gamma_e B_m$ denotes the mode's resonance frequency, with γ_e being the gyromagnetic ratio [58]. By quantizing the collective coordinates, the skyrmion can be treated as a qubit that can be controlled and manipulated. The energy levels of the \hat{S}_z skyrmion qubit are anharmonic, the effective Hamiltonian of the \hat{S}_z qubit within the subspace $\{|0\rangle, |1\rangle\}$ is given by $\hat{H}_{S_z} = \frac{K_0}{2} \hat{\sigma}_z - \frac{E_z}{2} \hat{\sigma}_x$ [58, 66, 98, 99]. The interaction Hamiltonian is given by $\hat{H}_{int} = \frac{\tilde{g}_{ms}}{2} (\hat{m} + \hat{m}^\dagger) \hat{\sigma}_x + \frac{g_{ms}}{2} (\hat{m} + \hat{m}^\dagger) \hat{\sigma}_z$ [58], where \tilde{g}_{ms} represents the coupling strength along the X and Y axes, and g_{ms} represents the coupling strength along the Z axis.

To achieve and dynamically control magnon blockade, we introduce a microwave drive applied to the skyrmion qubit with a driving frequency ω_s . The corresponding Hamiltonian is given by $H_s = \Omega_s \cos(\omega_s t) \hat{\sigma}_z$ [58]. Additionally, to observe the magnon blockade effect, a weak probe field is introduced into the system, with its Hamiltonian described as $H_d = \Omega_d (\hat{m}^\dagger e^{-i\omega_d t} + \hat{m} e^{i\omega_d t})$ [29, 100], where ω_d and Ω_d are the probe field's frequency and strength, respectively. The total Hamiltonian of the driven skyrmion qubit-magnon hybrid quantum system, therefore, is given by

$$\begin{aligned} \hat{H}_{total} = & \omega_m \hat{m}^\dagger \hat{m} + \frac{K_0}{2} \hat{\sigma}_z - \frac{E_z}{2} \hat{\sigma}_x \\ & + \frac{\tilde{g}_{ms}}{2} (\hat{m} + \hat{m}^\dagger) \hat{\sigma}_x + \frac{g_{ms}}{2} (\hat{m} + \hat{m}^\dagger) \hat{\sigma}_z \\ & + \Omega_s \cos(\omega_s t) \hat{\sigma}_z + \Omega_d (\hat{m}^\dagger e^{-i\omega_d t} + \hat{m} e^{i\omega_d t}). \end{aligned} \quad (1)$$

When the skyrmion qubit operates near the degeneracy point, its Hamiltonian \hat{H}_{S_z} can be expressed in terms of the eigenstates $|\psi_2\rangle = \frac{\sqrt{2}}{2} |1\rangle - \frac{\sqrt{2}}{2} |0\rangle$ and $|\psi_1\rangle = \frac{\sqrt{2}}{2} |1\rangle + \frac{\sqrt{2}}{2} |0\rangle$. In the subspace spanned by $\{|\psi_2\rangle, |\psi_1\rangle\}$, the Pauli operators are defined as $\tilde{\sigma}_z = |\psi_2\rangle\langle\psi_2| - |\psi_1\rangle\langle\psi_1|$ and $\tilde{\sigma}_x = |\psi_2\rangle\langle\psi_1| + |\psi_1\rangle\langle\psi_2|$, the coupling term \tilde{g}_{ms} does not induce transitions between energy levels; instead, it causes a minor shift in the energy levels of the skyrmion qubit. This shift is on the order of megahertz ($\tilde{g}_{ms} \approx 50.1$ MHz), which is considerably smaller than the gigahertz-scale resonant frequencies of the hybrid system ($E_z \approx \omega_m \approx 9.8$ GHz), therefore, this term can be neglected [58, 99]. Using the rotating-wave approximation (RWA) and considering the time-evolution operator in the rotating frame, $U = e^{-i(\frac{W_s \tilde{\sigma}_z t}{2} + \omega_d t \hat{m}^\dagger \hat{m})}$, the hybrid quantum system Hamiltonian can be simplified. Thus, the effective Hamiltonian can be written as

$$\begin{aligned} H_{eff} = & \Delta_m \hat{m}^\dagger \hat{m} + \frac{\Delta_s}{2} \tilde{\sigma}_z + \frac{g_{ms}}{2} (\hat{m} \tilde{\sigma}_+ + \hat{m}^\dagger \tilde{\sigma}_-) \\ & + \frac{\Omega_s}{2} (\tilde{\sigma}_+ + \tilde{\sigma}_-) + \Omega_d (\hat{m}^\dagger + \hat{m}), \end{aligned} \quad (2)$$

where $\Delta_m \equiv \omega_m - \omega_d$ ($\Delta_s \equiv E_z - \omega_s$) represents the detuning between the magnon mode and the probe field frequency, while Δ_s represents the detuning between the skyrmion qubit frequency and the driving frequency. The approximate con-

ditions are $\omega_d \approx \omega_s$, $\omega_d \gg g_{ms}$, and $\omega_s \gg \Omega_s$, with $\Delta = \Delta_s = \Delta_m$.

III. MAGNON BLOCKADE AND THE STEADY-STATE EQUAL-TIME SECOND-ORDER CORRELATION FUNCTION

A. the analytical expression for the steady-state equal-time second-order correlation function

In the weak-driving regime, where $\Omega_d, \Omega_s \ll k_m, k_s$, and the effects of quantum jumps on short time scales are neglected, the wave function of the composite system can be approximated within the framework of an analytical model [29, 30, 45–47, 50, 91, 101, 102]. Under this approximation, the system's dynamics can be effectively described by the master equation (Eq. (9)), which, in turn, is approximated by a non-Hermitian Hamiltonian. The non-Hermitian Hamiltonian governing the system is given by

$$\hat{H}_{\text{non}} = \hat{H}_{\text{eff}} - i\frac{k_m}{2}m^\dagger m - i\frac{k_s}{2}\tilde{\sigma}_+\tilde{\sigma}_- \quad (3)$$

thus, the Hilbert space of the composite system can be truncated to a subspace corresponding to a few excitations, and the system's evolution can be effectively approximated by a pure state, as described below

$$|\psi\rangle = C_{g0}|g0\rangle + C_{g1}|g1\rangle + C_{e0}|e0\rangle + C_{e1}|e1\rangle + C_{g2}|g2\rangle \quad (4)$$

where C_{ms} ($ms = g0, g1, e0, e1, g2$) are the probability amplitudes for the states $|ms\rangle$, and $|g(e), n\rangle$ represents the ground (excited) state of the Skyrmion qubit and the Fock state of the magnon mode, respectively.

Based on the Schrödinger equation $i\frac{d}{dt}|\psi(t)\rangle = \hat{H}_{\text{non}}|\psi(t)\rangle$, the dynamical evolution of the coefficients C_{ms} can be derived from the equations. The corresponding dynamical equations can then be written as

$$i\dot{C}_{g,0} = \frac{\Omega_s}{2}C_{e,0} + \Omega_d C_{g,1} \quad (5a)$$

$$i\dot{C}_{e,0} = (\Delta_s - i\frac{k_s}{2})C_{e,0} + \frac{g_{ms}}{2}C_{g,1} + \frac{\Omega_s}{2}C_{g,0} \quad (5b)$$

$$i\dot{C}_{g,1} = (\Delta_m - i\frac{k_m}{2})C_{g,1} + \frac{g_{ms}}{2}C_{e,0} + \Omega_d C_{g,0} \quad (5c)$$

$$i\dot{C}_{e,1} = (\Delta_m + \Delta_s - i\frac{k_m}{2} - i\frac{k_s}{2})C_{e,1} + \frac{\sqrt{2}}{2}g_{ms}C_{g,2} + \frac{\Omega_s}{2}C_{g,1} + \Omega_d C_{e,0} \quad (5d)$$

$$i\dot{C}_{g,2} = (\Delta_m - i\frac{k_m}{2})C_{g,2} + \sqrt{2}\Omega_d C_{g,1} + \frac{\sqrt{2}}{2}g_{ms}C_{e,1} \quad (5e)$$

then its steady-state solution can be obtained from

$$0 = \frac{\Omega_s}{2}C_{e,0} + \Omega_d C_{g,1}, \quad (6a)$$

$$0 = (\Delta_s - i\frac{k_s}{2})C_{e,0} + \frac{g_{ms}}{2}C_{g,1} + \frac{\Omega_s}{2}C_{g,0}, \quad (6b)$$

$$0 = (\Delta_m - i\frac{k_m}{2})C_{g,1} + \frac{g_{ms}}{2}C_{e,0} + \Omega_d C_{g,0}, \quad (6c)$$

$$0 = (\Delta_m + \Delta_s - i\frac{k_m}{2} - i\frac{k_s}{2})C_{e,1} + \frac{\sqrt{2}}{2}g_{ms}C_{g,2} + \frac{\Omega_s}{2}C_{g,1} + \Omega_d C_{e,0}, \quad (6d)$$

$$0 = (\Delta_m - i\frac{k_m}{2})C_{g,2} + \sqrt{2}\Omega_d C_{g,1} + \frac{\sqrt{2}}{2}g_{ms}C_{e,1}. \quad (6e)$$

In the weak-driving regime, where $\Omega_d, \Omega_s \ll k_m, k_s$, the following relationships hold: $|C_{g,0}| \gg |C_{g,1}|, |C_{g,2}|, |C_{e,0}| \gg |C_{g,3}|, |C_{e,1}|, |C_{e,2}|$. By applying perturbation theory, we neglect the higher-order terms that contribute minimally in the equation of motion for the lower-order variables. We can derive the steady-state solutions for the probability amplitudes

$$C_{g,0} \approx 1 \quad (7a)$$

$$C_{e,0} = \frac{-2\Omega_d g_{ms} + 2\tilde{\Delta}_m \Omega_s}{-4\tilde{\Delta}_m \tilde{\Delta}_s + g_{ms}^2} \quad (7b)$$

$$C_{g,1} = \frac{4\tilde{\Delta}_s \Omega_d - \Omega_s g_{ms}}{-4\tilde{\Delta}_m \tilde{\Delta}_s + g_{ms}^2} \quad (7c)$$

$$C_{e,1} = \frac{-\Omega_s D A - 2A \Omega_d E + 8\tilde{\Delta}_s \Omega_d g_{ms} - 2g_{ms}^2 \Omega_d \Omega_s}{(-4\tilde{\Delta}_m \tilde{\Delta}_s + g_{ms}^2)(2AB - g_{ms}^2)} \quad (7d)$$

$$C_{g,2} = \frac{-2\sqrt{2}BC + \Omega_s D g_{ms} + 2\Omega_d E g_{ms}}{(-4\tilde{\Delta}_m \tilde{\Delta}_s + g_{ms}^2)(2\sqrt{2}AB - \sqrt{2}g_{ms}^2)} \quad (7e)$$

where $\tilde{\Delta}_m = \Delta - i\frac{k_m}{2}$, $\tilde{\Delta}_s = \Delta - i\frac{k_s}{2}$, $A = 2(\Delta - i\frac{k_m}{2})$, $B = (2\Delta - i\frac{k_m}{2} - i\frac{k_s}{2})$, $C = 4\sqrt{2}\tilde{\Delta}_s \Omega_d^2 - \sqrt{2}g_{ms} \Omega_d \Omega_s$, $D = 4\tilde{\Delta}_s \Omega_d - \Omega_s g_{ms}$, $E = -2\Omega_d g_{ms} + 2\tilde{\Delta}_m \Omega_s$.

With the steady-state amplitudes in Eqs. (7c) and (7e), the function $g^{(2)}$ can then be expressed by

$$g^{(2)}(0) \approx \frac{2|C_{g2}|^2}{|C_{g1}|^4} = \frac{2|\eta_1|^2 \cdot |\chi|^2}{|\eta_2|^2 |D|^4} \quad (8)$$

in which $\eta_1 = -2\sqrt{2}BC + \Omega_s D g_{ms} + 2\Omega_d E g_{ms}$, $\eta_2 = 2\sqrt{2}AB - \sqrt{2}g_{ms}^2$, $\chi = -4\tilde{\Delta}_m \tilde{\Delta}_s + g_{ms}^2$.

B. Numerical Simulation of the Second-Order Correlation Function

Considering the damping effects induced by the system-bath coupling, the dissipative dynamics of the hybrid skyrmion qubit-magnon system, with a focus on the magnon

mode, can be described by the master equation [94]

$$\begin{aligned} \frac{\partial \rho}{\partial t} = & -i[H_{\text{eff}}, \rho] + \frac{\kappa_m}{2}(n_{\text{th}} + 1)\mathcal{L}_m[\rho] \\ & + \frac{\kappa_m}{2}n_{\text{th}}\mathcal{L}'_m[\rho] + \frac{\kappa_s}{2}\mathcal{L}_{\tilde{\sigma}}[\rho], \end{aligned} \quad (9)$$

here, κ_s and κ_m represent the decay rates of the skyrmion qubit and the magnon mode, respectively. The Pauli operators are defined as $\tilde{\sigma}_+ = |\psi_2\rangle\langle\psi_1|$ and $\tilde{\sigma}_- = |\psi_1\rangle\langle\psi_2|$, where $|\psi_1\rangle$ and $|\psi_2\rangle$ are the eigenstates of the skyrmion qubit. For simplicity, we assume $\kappa_s = \kappa_m$, where ρ is the system density matrix. The Lindblad superoperators are defined as follows

$$\mathcal{L}_m[\rho] = 2m\rho m^\dagger - m^\dagger m\rho - \rho m^\dagger m, \quad (10)$$

$$\mathcal{L}_{\tilde{\sigma}}[\rho] = 2\tilde{\sigma}_-\rho\tilde{\sigma}_+ - \tilde{\sigma}_+\tilde{\sigma}_-\rho - \rho\tilde{\sigma}_+\tilde{\sigma}_-. \quad (11)$$

The phenomenon of magnon blockade can be quantified using the second-order correlation function, given by [103]

$$g^{(2)}(0) = \frac{\text{Tr}(\rho m^\dagger m^\dagger m m)}{[\text{Tr}(\rho m^\dagger m)]^2} = \frac{\langle m^\dagger m^\dagger m m \rangle}{\langle m^\dagger m \rangle^2}. \quad (12)$$

The second-order correlation function $g^{(2)}(0)$ can be numerically obtained by solving the master equation given in Eq. (9) using Monte Carlo wave function simulation [104], alongside the effective Hamiltonian H_{eff} from Eq. (2). If $g^{(2)}(0) > 1$, this indicates that the steady-state magnon number distribution follows super-Poissonian statistics, exhibiting magnon bunching. Conversely, if $0 < g^{(2)}(0) < 1$, the magnon number distribution satisfies sub-Poissonian statistics, known as magnon antibunching [87–89]. Specifically, when $g^{(2)}(0) \rightarrow 0$, magnon blockade occurs. In our scheme, the second-order correlation function can be as low as $g^{(2)}(0) \rightarrow 10^{-6}$, which is a strong indication of magnon blockade [29, 100, 105]. Therefore, our study provides theoretical support for the generation of a single-photon source, which is significant for investigating fundamental aspects of quantum magnons and for potential applications in magnon-based quantum simulation and hybrid quantum devices [13, 58, 106].

In our simulation, we examine how the equal-time second-order correlation function depends on various system parameters, such as the driving detuning, the effective qubit-magnon coupling strength, the dissipation rates of the magnon mode and the skyrmion-qubit, and the thermal magnon occupation number, decay rate.

In Fig. 2(a), the steady-state second-order correlation function $\log_{10} g^{(2)}(0)$ varies with the drive detuning Δ/γ and the coupling strength g_{ms}/γ between the magnon and the skyrmion-qubit. The color gradient from deep purple to yellow represents the transition of $g^{(2)}(0)$ from strong quantum correlations to classical correlations. Near the white dashed lines, the drive detuning is approximately half of the coupling strength, i.e., $\Delta/\gamma \approx \pm \frac{1}{2}g_{ms}/\gamma$, at which point $g^{(2)}(0)$ reaches its minimum, indicating significant antibunching and a pronounced magnon blockade effect in the system. The relationship between the second-order correlation function $g^{(2)}(0)$ and the control field strength Ω_s/γ , as well as the probe field strength Ω_d/γ , is shown in Fig. 2(b). As Ω_s/γ and

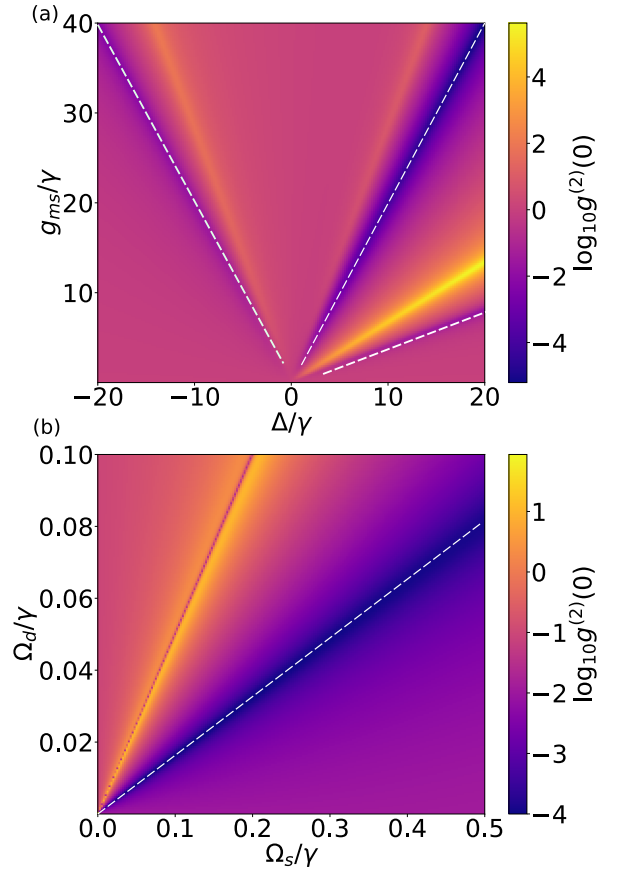


FIG. 2. The variation of the steady-state equal-time second-order correlation function $\log_{10} g^{(2)}(0)$ is plotted varies with (a) as a function of the driving detuning Δ/γ and the skyrmion qubit-magnon coupling strength g_{ms}/γ , and (b) as a function of the control field strength Ω_s/γ and the probe field strength Ω_d/γ . To maintain consistency throughout the paper, all frequencies are scaled using $\gamma = 2\pi \times 1$ MHz. In (a), $\Omega_s/\gamma = 0.06$ and $\Omega_d/\gamma = 0.01$, while in (b), $\Delta/\gamma = 10$ and $g_{ms}/\gamma = 19.6$. The other system parameters are $\kappa_m/\gamma = \kappa_q/\gamma = 1$, and $n_{\text{th}} = 0$.

Ω_d/γ increase, $g^{(2)}(0)$ exhibits significant changes. Notably, $g^{(2)}(0)$ reaches its minimum near the white dashed lines, suggesting the possibility of achieving magnon blockade by appropriately tuning the external driving fields.

It is essential to clearly state that the detection field and the driving field are indispensable for enhancing magnon blockade. In Fig. 3, we explore the optimal connection between the coupling strength g_{ms} , the optimal driving field strength Ω_s , and the dissipation rate κ . In Fig. 3(a), at high coupling strength g_{ms} and low dissipation rate κ , $\log_{10} g^{(2)}(0)$ remains at a low value (deep purple), with a magnitude less than 10^{-8} , indicating a strong antibunching effect. We fixed a strong coupling strength $g_{ms}/\gamma = 19.6$ and optimized the $g^{(2)}(0)$ function by adjusting the parameter space of Ω_s and κ , as shown in Fig. 3(b). Our goal is to identify the optimal driving strength and dissipation range under this coupling strength. When Ω_s/γ approaches 0.06, $\log_{10} g^{(2)}(0)$ shows a clear low-value region (deep purple band), particularly in the range of κ/γ from 0 to 0.6, indicating that at this

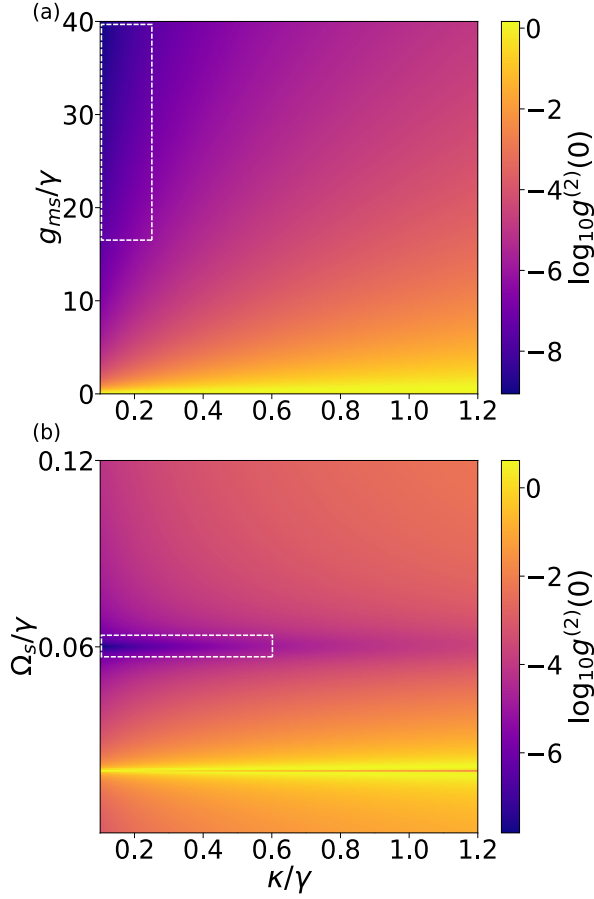


FIG. 3. The steady-state $\log_{10} g^{(2)}(0)$ is plotted as a function of (a) the coupling strength g_{ms} and (b) the control field strength Ω_s/γ , as well as the dissipation rate κ , under the condition $\Delta/\gamma \approx \frac{1}{2}g_{ms}/\gamma$. In (a), $\Omega_s/\gamma = 0.06$ and $\Omega_d/\gamma = 0.01$, while in (b) $g_{ms}/\gamma = 19.6$, and $n_{th} = 0$.

driving field strength, the second-order correlation function reaches its minimum, and the magnon blockade effect is most pronounced. Interestingly, there exists a well-defined optimal driving field strength, detection field strength, and a specific dissipation range to maximize the magnon blockade effect.

Next, we observe that the second-order correlation function $g^{(2)}(0)$ exhibits a strong dependence on the driving detuning, with clearer results presented in Fig. 4. The optimal dissipation region k is selected with $k/\gamma = 0.15$. Specifically, we plot the second-order correlation function $g^{(2)}(0)$ as a function of the driving detuning Δ/γ . The variation of $g^{(2)}(0)$ with detuning Δ/γ for different magnon driving field strengths ($\Omega_d/\gamma = 0.004, 0.01, 0.012$) is shown in Fig. 4(a), where the skyrmion driving field is kept constant at $\Omega_s/\gamma = 0.06$. As expected, a strong antibunching effect is observed around $\Delta/\gamma \approx 10$, indicating a pronounced magnon blockade effect. In this range, the antibunching effect is sensitive to modulation of the probe and driving fields. However, it is also observed that the antibunching effect around $\Delta/\gamma \approx -10$ is less sensitive to such modulation. When $\Omega_d/\gamma = 0.01$, the system displays the strongest antibunching effect, with $g^{(2)}(0)$ ap-

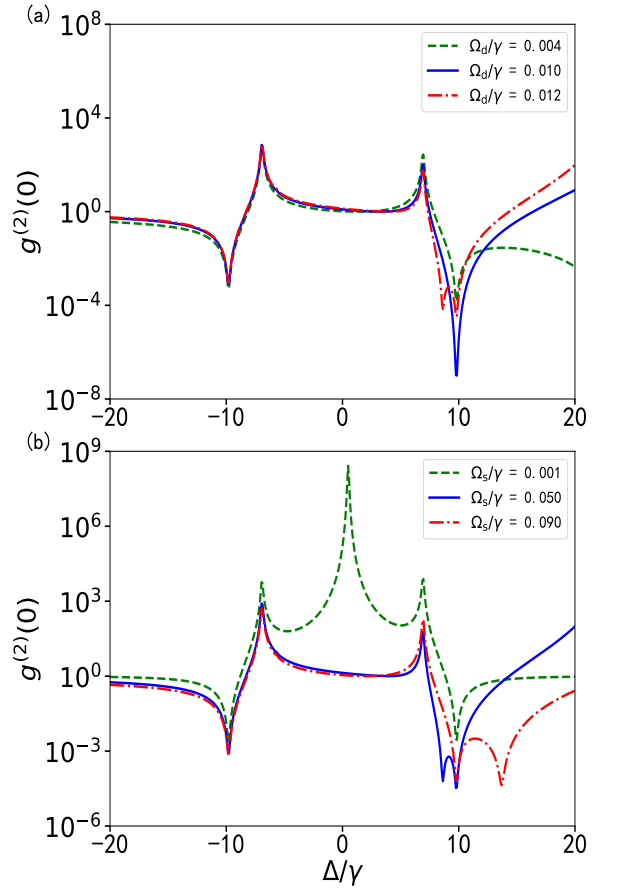


FIG. 4. The equal-time second-order correlation function $g^{(2)}(0)$ is shown as a function of the normalized detuning Δ/γ . As illustrated in (a), for the magnon drive field strengths $\Omega_d/\gamma = 0.004, 0.01$, and 0.012 , the Skyrmion drive field Ω_s/γ is kept constant at 0.06 . In (b), for the skyrmion drive field strengths $\Omega_s/\gamma = 0.001, 0.05$, and 0.09 , the magnon drive field Ω_d/γ is fixed at 0.01 . The coupling strength between the magnon and skyrmion modes is $g_{ms}/\gamma = 19.6$. The other system parameters are $\kappa_m/\gamma = \kappa_q/\gamma = 0.15$, and $n_{th} = 0$.

proaching 10^{-6} . In Fig. 4(b), the dependence of $g^{(2)}(0)$ on the skyrmion driving field strengths ($\Omega_s/\gamma = 0.001, 0.05, 0.09$) is shown, while the magnon driving field remains fixed at $\Omega_d/\gamma = 0.05$. Similar to the magnon driving fields, the strongest antibunching effect is observed at $\Omega_s/\gamma = 0.05$, where $g^{(2)}(0)$ approaches 10^{-5} , indicating optimal suppression of paired magnon excitations.

In Fig. 5, the relationships among Ω_d , g_{ms} , Ω_s , and κ are more clearly demonstrated. It shows that the system exhibits the strongest antibunching effect around $\Omega_s/\gamma \approx 0.06$ and $\Omega_d/\gamma \approx 0.01$. A lower decay rate ($\kappa/\gamma = 0.15$) helps the system maintain a stronger antibunching effect, as indicated by the lower value of $g^{(2)}(0)$. As the decay rate increases, the antibunching effect weakens, but even at higher dissipation, $\log_{10} g^{(2)}(0)$ still reaches a good magnitude.

Finally considering a bosonic environment at nonzero temperature, we can analyze the impact of ambient thermal noise on the magnon blockade. Fig. 6 illustrates the significant dependence of the second-order correlation function $g^{(2)}(0)$ on

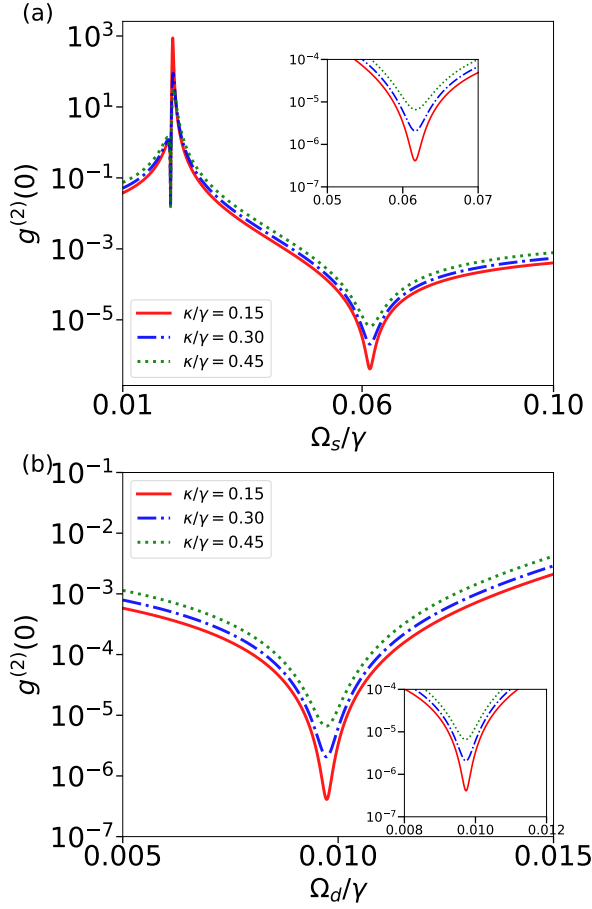


FIG. 5. The dependence of the second-order correlation function $g^{(2)}(0)$ on both the skyrmion driving field Ω_s/γ and the magnon driving field Ω_d/γ . In (a), $g^{(2)}(0)$ is plotted as a function of Ω_s/γ for detuning values $\kappa/\gamma = 0.15$, $\kappa/\gamma = 0.3$, and $\kappa/\gamma = 0.45$, $\Omega_d/\gamma = 0.01$. In (b), the behavior of $g^{(2)}(0)$ is depicted as a function of Ω_d/γ under the same detuning conditions, $\Omega_s/\gamma = 0.06$, while the other parameters are the same as those in Fig. 4.

the coupling strength g_{ms}/γ , exhibiting different behaviors under various thermal magnon occupation numbers n_{th} . By numerically solving the master equation, we plotted the variation of $g^{(2)}(0)$ as a function of the qubit-magnon coupling strength g_{ms}/γ for different thermal magnon occupation numbers $n = (0, 10^{-8}, 10^{-7})$. With $g_{ms} = 19.6$, the results show that the thermal magnon number significantly affects the magnon blockade effect. When $n_{th} = 0$ (red solid line), the second-order correlation function reaches its minimum value, around 10^{-6} , near $g_{ms}/\gamma \approx 20$, indicating that the system is in a strong blockade regime, where magnon excitations are significantly suppressed. For $n_{th} = 10^{-8}$, $n_{th} = 10^{-7}$, and $n_{th} = 10^{-6}$ (green dashed line, blue dashed line, and purple dashed line, respectively), the magnon blockade effect is disrupted as the thermal magnon occupation number increases. Although antibunching behavior can still be observed near $g_{ms}/\gamma \approx 20$, the minimum value increases compared to the zero thermal occupation case, indicating that the presence of thermal magnons weakens the blockade ef-

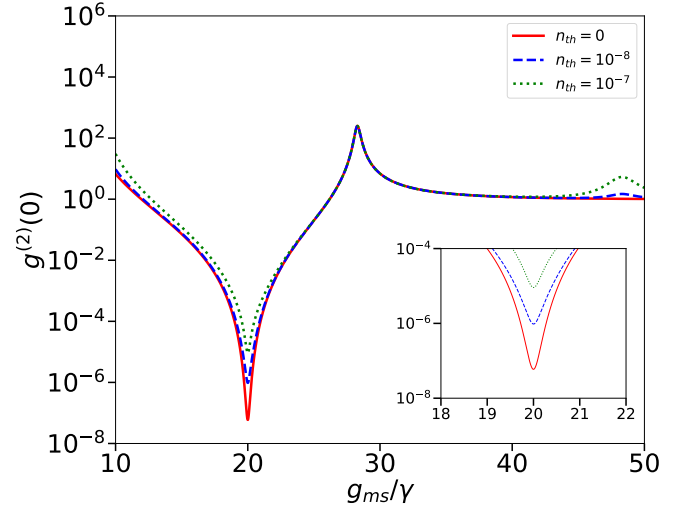


FIG. 6. The equal-time second-order correlation function $g^{(2)}(0)$ is plotted as a function of the effective skyrmion qubit-magnon coupling strength g_{ks}/γ under different thermal noise occupation numbers $n_{th} = (0, 10^{-8}, 10^{-7})$. The parameters used in this calculation are $(\Delta, \Omega_s, \Omega_d)/\gamma = (10, 0.06, 0.01)$, while the other parameters are the same as those in Fig. 4.

fect. Thus, for a more pronounced observation of the magnon blockade, the YIG material must be cooled to low temperatures. The thermal magnon occupation number is given by $n_{th} = \left[\exp\left(\frac{\hbar\omega_m}{k_B T}\right) - 1 \right]^{-1}$, where $\omega_m = 9.8$ GHz. At temperatures of 4.06mK, 4.64mK, the corresponding thermal occupation numbers are 10^{-8} , 10^{-7} , respectively. This figure demonstrates that adjusting both the thermal magnon occupation number n_{th} and the coupling strength effectively controls the magnon blockade effect, influencing multi-particle excitations in the magnon mode, which is crucial for the design of quantum information processing and quantum control systems.

IV. DISCUSSIONS

In the skyrmion-qubit system, information is stored in the quantum degree of helicity, and the logical states can be controlled by electric and magnetic fields, as reflected in K_0 and E_z , respectively[66].

For the case discussed above, where $E_z \approx 9.8$ GHz and $K_0 \approx 0$, the computed $g^{(2)}(0)$ as a function of detuning, derived from numerical simulations under various driving strengths, demonstrates excellent agreement with the corresponding analytical predictions. This concordance substantiates the validity of the approximations employed in the theoretical framework. Furthermore, the absence of instability effects arising from small dissipation provides additional confirmation of the robustness of the adopted approximation.

In addition, for the scenario where $E_z \approx 0$ and $K_0 \approx 9.8$ GHz, the system is configured to exclusively drive the magnon mode, while the external driving on the skyrmion

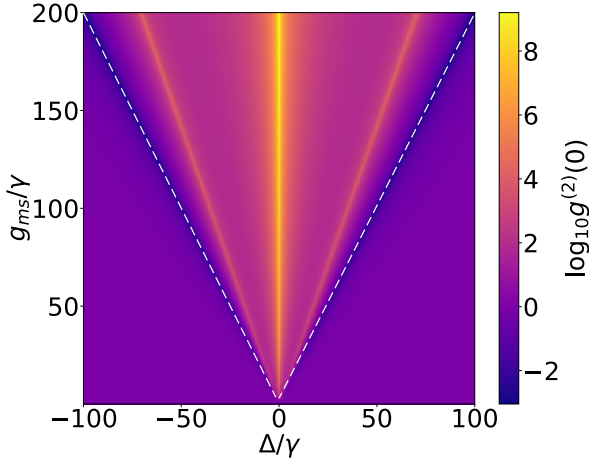


FIG. 7. The variation of the steady-state equal-time second-order correlation function $\log_{10} g^{(2)}(0)$ is shown as a function of the driving detuning Δ/γ and the skyrmion qubit-magnon coupling strength g_{ms}/γ . The probe field strength of the magnons is fixed at $\Omega_d/\gamma = 0.01$, while other system parameters are set to $\kappa_m/\gamma = \kappa_q/\gamma = 1$.

qubit is removed. The skyrmion is instead modulated via external magnetic and electric fields, with the modulation explicitly affecting the parameters K_0 and E_z . The Hamiltonian is written as

$$\begin{aligned} \hat{H}'_{\text{total}} = & \omega_m \hat{m}^\dagger \hat{m} + \frac{K_0}{2} \hat{\sigma}_z + \frac{\tilde{g}_{ms}}{2} (\hat{m} + \hat{m}^\dagger) \hat{\sigma}_x \\ & + \frac{g_{ms}}{2} (\hat{m} + \hat{m}^\dagger) \hat{\sigma}_z + \Omega_d (\hat{m}^\dagger e^{-i\omega_d t} + \hat{m} e^{i\omega_d t}). \end{aligned} \quad (13)$$

The coupling term \tilde{g}_{ms} induces transitions between energy levels, with the coupling strength ranging from 50.1 MHz to 200 MHz, whereas the coupling term g_{ms} causes a small shift in the energy levels of the skyrmion qubit, with the shift ranging from 19.6 MHz to 36 MHz [58]. This shift is significantly smaller than the resonance frequencies of the hybrid system ($K_0 \approx \omega_m \approx 9.8$ GHz), and therefore, this term can be neglected. By employing the rotating-wave approximation (RWA), the Hamiltonian of the hybrid quantum system can be simplified. The effective Hamiltonian can then be written as

$$\begin{aligned} \hat{H}'_{\text{eff}} = & \Delta_m \hat{m}^\dagger \hat{m} + \frac{\Delta_s}{2} \hat{\sigma}_z + \frac{g_{ms}}{2} (\hat{m} \hat{\sigma}_+ + \hat{m}^\dagger \hat{\sigma}_-) \\ & + \Omega_d (\hat{m}^\dagger + \hat{m}), \end{aligned} \quad (14)$$

where $\Delta_m \equiv \omega_m - \omega_d$ ($\Delta_s \equiv K_0 - \omega_d$) represents the detuning between the magnon mode and the driving field frequency, while Δ_s represents the detuning between the skyrmion qubit frequency and the driving frequency. Simultaneously, $\Delta = \Delta_s = \Delta_m$. The master equation is expressed as follows[94]

$$\frac{\partial \rho}{\partial t} = -i[H_{\text{eff}}, \rho] + \frac{\kappa_m}{2} \mathcal{L}_m[\rho] + \frac{\kappa_s}{2} \mathcal{L}_\sigma[\rho], \quad (15)$$

the dissipator is defined as the Lindblad superoperators $\mathcal{L}[\rho] = 2o\rho o^\dagger - o^\dagger \rho o - \rho o^\dagger o$, with $o = \hat{m}, \hat{\sigma}_-$ indicating, respectively.

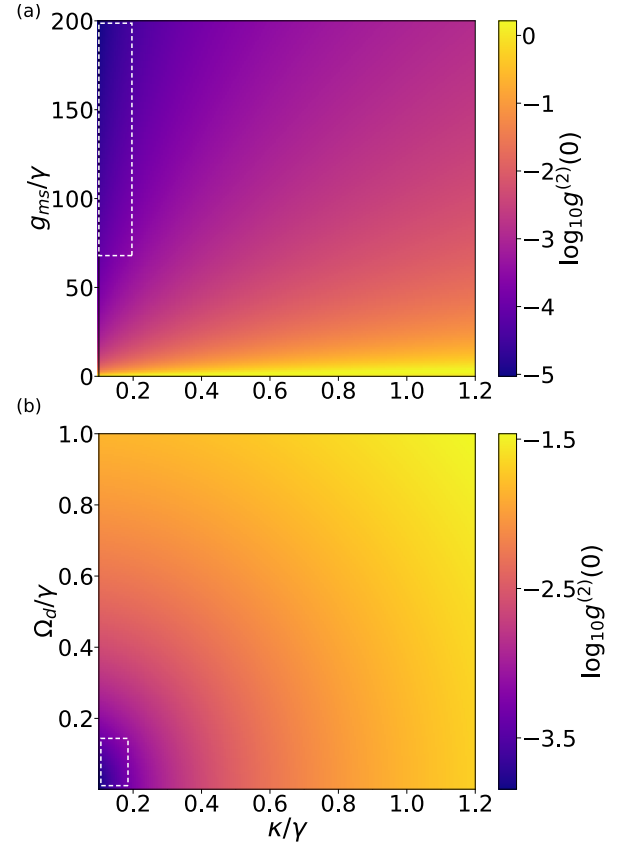


FIG. 8. The steady-state $\log_{10} g^{(2)}(0)$ is presented as a function of (a) the skyrmion-qubit coupling strength g_{ms} and (b) the control field strength Ω_d/γ , along with the dissipation rate κ , under the condition $\Delta/\gamma \approx \frac{1}{2} g_{ms}/\gamma$. In panel (a), $\Omega_d/\gamma = 0.01$ is set, while in panel (b), $g_{ms}/\gamma = 50.1$ is chosen, while the other parameters are the same as those in Fig. 7.

The Fig. 7 shows the variation of the steady-state equal-time second-order correlation function $\log_{10} g^{(2)}(0)$ as a function of the driving detuning Δ/γ and the skyrmion qubit-magnon coupling strength g_{ms}/γ . It can also be observed that under the optimal conditions where $\Delta/\gamma \approx \pm \frac{1}{2} g_{ms}/\gamma$, $\log_{10} g^{(2)}(0)$ reaches -2, indicating the occurrence of a strong magnon blockade effect. This results in a symmetric relationship, which differs slightly from the case where two drives are applied simultaneously.

In the analysis of Fig. 8(a), we investigate the effects of the dissipation rate k and the Skyrmion qubit-magnon coupling strength g_{ms} on the system's behavior. The results show that, for higher coupling strengths and lower dissipation rates k , the logarithmic value of the second-order correlation function $\log_{10} g^{(2)}(0)$ remains at a relatively low value (around -5), consistent with the two driving influences acting on the system. In Fig. 8(b), we further examine the impact of the driving strength Ω_d on the system. When the dissipation rate k is fixed, small variations in the driving strength (e.g., $0.001 \leq \Omega_d \leq 0.01$) do not significantly affect the system, and the logarithmic value of the second-order correlation function $\log_{10} g^{(2)}(0)$ remains stable. However, when

the driving strength undergoes a large variation, the system exhibits pronounced fluctuations, and the second-order correlation function shows significant changes, with a marked enhancement of the magnon blockade effect. Notably, even when no external drive is applied to the Skyrmion qubit, the application of a drive solely to the magnons effectively induces a magnon blockade effect.

V. CONCLUSION

We propose a scheme to realize a controlled magnon blockade effect in a hybrid skyrmion-magnon system. By numerically solving the quantum master equation describing the system's Hamiltonian, we found the statistical properties of the magnon mode, particularly observing a pronounced magnon blockade effect through the second-order correlation function $g^{(2)}(0)$. We consider two scenarios: one where both the magnon and the skyrmion are driven, with $E_z \approx 9.8$ GHz and $K_0 \approx 0$, and another where only the magnon is driven, with $E_z \approx 0$ and $K_0 \approx 9.8$ GHz.

In the first scenario, where both the magnon and skyrmion are driven and the skyrmion is modulated by a magnetic field, we can effectively control $g^{(2)}(0)$ by adjusting the coupling strength g_{ms} and the driving fields Ω_s or Ω_d , leading to the observation of quantum antibunching phenomena. The model supports the realization of magnon blockade across a wide

range of coupling strengths and external driving fields. The coupling strength between the skyrmion qubit and the magnon mode is directly influenced by the vertical distance between the skyrmion and the surface and center of the YIG sphere, with a maximum coupling strength of up to 40 MHz [58]. Under these conditions, when the thermal magnon occupation number is $n_{th} = 0$, the second-order correlation function $g^{(2)}(0)$ can be reduced to the order of 10^{-7} .

In the second scenario, where only the magnon is driven and the skyrmion is modulated by a magnetic field, the coupling strength g_{ms} can reach up to 200 MHz [58]. By appropriately tuning the coupling strength g_{ms} and the driving field Ω_d , the magnon blockade effect is also observed. Further analysis of the system's dissipation, driving fields shows that, under suitable parameter settings, the magnon blockade effect is still observed, with $g^{(2)}(0)$ reaching approximately 10^{-2} . We believe that with further optimization and experimental validation, this scheme will provide a theoretical foundation for the potential application of single-magnon emitters.

ACKNOWLEDGMENTS

We thank Feng-Yang Zhang, Yexiong Zeng, and Ye-Ting Yan for constructive discussions. This work was supported by the National Natural Science Foundation of China (Grants No. 12274053).

-
- [1] M. Wallquist, K. Hammerer, P. Rabl, M. Lukin, and P. Zoller, Hybrid quantum devices and quantum engineering, *Phys. Scr.* **T137**, 014001 (2009).
 - [2] H. J. Kimble, The quantum internet, *Nature* **453**, 1023 (2008).
 - [3] Z.-L. Xiang, S. Ashhab, J. Q. You, and F. Nori, Hybrid quantum circuits: Superconducting circuits interacting with other quantum systems, *Rev. Mod. Phys.* **85**, 623 (2013).
 - [4] G. Kurizki, P. Bertet, Y. Kubo, K. Mølmer, D. Petrosyan, P. Rabl, and J. Schmiedmayer, Quantum technologies with hybrid systems, *Proc. Natl. Acad. Sci. U.S.A.* **112**, 3866 (2015).
 - [5] A. A. Serga, A. V. Chumak, and B. Hillebrands, YIG magnonics, *J. Phys. D: Appl. Phys.* **43**, 264002 (2010).
 - [6] A. V. Chumak, V. I. Vasyuchka, and B. Serga, A. A. and Hillebrands, Magnon spintronics, *Nat. Phys.* **11**, 453 (2015).
 - [7] S. Zheng, Z. Wang, Y. Wang, F. Sun, Q. He, P. Yan, and H. Y. Yuan, Tutorial: Nonlinear magnonics, *J. Appl. Phys.* **134**, 151101 (2023).
 - [8] H. Y. Yuan, Y. Cao, A. Kamra, R. A. Duine, and P. Yan, Quantum magnonics: When magnon spintronics meets quantum information science, *Phys. Rep.* **965**, 1 (2022).
 - [9] B. Z. Rameshti, S. V. Kusminskiy, J. A. Haigh, K. Usami, D. Lachance-Quirion, Y. Nakamura, C.-M. Hu, H. X. Tang, G. E. W. Bauer, and Y. M. Blanter, Cavity Magnonics, *Phys. Rep.* **979**, 1 (2022).
 - [10] H. J. Kimble, The quantum internet, *Nature(London)* **453**, 1023 (2008).
 - [11] H. Huebl, C. W. Zollitsch, J. Lotze, F. Hocke, M. Greifenstein, A. Marx, R. Gross, and S. T. B. Goennenwein, High Cooperativity in Coupled Microwave Resonator Ferrimagnetic Insulator Hybrids, *Phys. Rev. Lett.* **111**, 127003 (2013).
 - [12] Y. Tabuchi, S. Ishino, T. Ishikawa, R. Yamazaki, K. Usami, and Y. Nakamura, Hybridizing Ferromagnetic Magnons and Microwave Photons in the Quantum Limit, *Phys. Rev. Lett.* **113**, 083603 (2014).
 - [13] Y. Li, T. Polakovic, Y.-L. Wang, J. Xu, S. Lendinez, Z. Zhang, J. Ding, T. Khaire, H. Saglam, R. Divan, J. Pearson, W.-K. Kwok, Z. Xiao, V. Novosad, A. Hoffmann, and W. Zhang, Strong Coupling between Magnons and Microwave Photons in On-Chip Ferromagnet-Superconductor Thin-Film Devices, *Phys. Rev. Lett.* **123**, 107701 (2019).
 - [14] Y.-P. Wang, G.-Q. Zhang, D. Zhang, X.-Q. Luo, W. Xiong, S.-P. Wang, T.-F. Li, C.-M. Hu, and J. Q. You, Magnon Kerr effect in a strongly coupled cavity-magnon system, *Phys. Rev. B* **94**, 224410 (2016).
 - [15] J. Chen, X.-G. Fan, W. Xiong, D. Wang, and L. Ye, Nonreciprocal entanglement in cavity-magnon optomechanics, *Phys. Rev. B* **108**, 024105 (2023).
 - [16] W. Xiong, M. Wang, G.-Q. Zhang, and J. Chen, Optomechanical-interface-induced strong spin-magnon coupling, *Phys. Rev. A* **107**, 033516 (2023).
 - [17] X. Zuo, Z.-Y. Fan, H. Qian, M.-S. Ding, H. Tan, H. Xiong, and J. Li, Cavity magnomechanics: from classical to quantum, *New Journal of Physics* **26**, 031201 (2024).
 - [18] A. Osada, R. Hisatomi, A. Noguchi, Y. Tabuchi, R. Yamazaki, K. Usami, M. Sadgrove, R. Yalla, M. Nomura, and Y. Nakamura, Cavity Optomagnonics with Spin-Orbit Coupled Photons, *Phys. Rev. Lett.* **116**, 223601 (2016).
 - [19] S. P. Wolski, D. Lachance-Quirion, Y. Tabuchi, S. Kono, A. Noguchi, K. Usami, and Y. Nakamura, Dissipation-Based Quantum Sensing of Magnons with a Superconducting Qubit,

- Phys. Rev. Lett.* **125**, 117701 (2020).
- [20] L. Trifunovic, F. L. Pedrocchi, and D. Loss, Long-Distance Entanglement of Spin Qubits via Ferromagnet, *Phys. Rev. X* **3**, 041023 (2013).
- [21] M. Fukami, D. R. Candido, D. D. Awschalom, and M. E. Flatté, Opportunities for Long-Range Magnon-Mediated Entanglement of Spin Qubits via On- and Off-Resonant Coupling, *Phys. Rev. X Quantum* **2**, 040314 (2021).
- [22] X. Zhang, C.-L. Zou, L. Jiang, and H. X. Tang, Cavity magnomechanics, *Sci. Adv.* **2**, e1501286 (2016).
- [23] Z. Shen, G.-T. Xu, M. Zhang, Y.-L. Zhang, Y. Wang, C.-Z. Chai, C.-L. Zou, G.-C. Guo, and C.-H. Dong, Coherent Coupling between Phonons, Magnons, and Photons, *Phys. Rev. Lett.* **129**, 243601 (2022).
- [24] M. Mergenthaler, J. Liu, J. J. Le Roy, N. Ares, A. L. Thompson, L. Bogani, F. Luis, S. J. Blundell, T. Lancaster, A. Ardavan, G. A. D. Briggs, P. J. Leek, and E. A. Laird, Strong Coupling of Microwave Photons to Antiferromagnetic Fluctuations in an Organic Magnet, *Phys. Rev. Lett.* **119**, 147701 (2017).
- [25] D. Xu, X.-K. Gu, H.-K. Li, Y.-C. Weng, Y.-P. Wang, J. Li, H. Wang, S.-Y. Zhu, and J. Q. You, Quantum Control of a Single Magnon in a Macroscopic Spin System, *Phys. Rev. Lett.* **130**, 193603 (2023).
- [26] A. Osada, A. Gloppe, R. Hisatomi, A. Noguchi, R. Yamazaki, M. Nomura, Y. Nakamura, and K. Usami, Brillouin Light Scattering by Magnetic Quasivortices in Cavity Optomagnonics, *Phys. Rev. Lett.* **120**, 133602 (2018).
- [27] T. S. Parvini, V. A. S. V. Bittencourt, and S. V. Kusminskiy, Antiferromagnetic cavity optomagnonics, *Phys. Rev. Res.* **2**, 022027 (2020).
- [28] M. Kounalakis, G. E. W. Bauer, and Y. M. Blanter, Analog Quantum Control of Magnonic Cat States on a Chip by a Superconducting Qubit, *Phys. Rev. Lett.* **129**, 037205 (2022).
- [29] Z.-X. Liu, H. Xiong, and Y. Wu, Magnon blockade in a hybrid ferromagnet-superconductor quantum system, *Phys. Rev. B* **100**, 134421 (2019).
- [30] J.-k. Xie, S.-l. Ma, and F.-l. Li, Quantum-interference-enhanced magnon blockade in an yttrium-iron-garnet sphere coupled to superconducting circuits, *Phys. Rev. A* **101**, 042331 (2020).
- [31] T.-X. Lu, H. Zhang, Q. Zhang, and H. Jing, Exceptional-point-engineered cavity magnomechanics, *Phys. Rev. A* **103**, 063708 (2021).
- [32] X. Wang, K.-W. Huang, and H. Xiong, Nonreciprocal sideband responses in a spinning microwave magnomechanical system, *Opt. Express* **31**, 5492 (2023).
- [33] H. Xiong, Magnonic frequency combs based on the resonantly enhanced magnetostrictive effect, *Fundam. Res.* **3**, 8 (2023).
- [34] D. Mukhopadhyay, J. M. P. Nair, and G. S. Agarwal, Quantum amplification of spin currents in cavity magnonics by a parametric drive induced long-lived mode, *Phys. Rev. B* **106**, 184426 (2022).
- [35] Y. Liu, A. Bergman, A. Bagrov, A. Delin, D. Thonig, M. Pereiro, O. Eriksson, S. Streib, E. Sjöqvist, and V. Azimi-Mousolou, Tunable phonon-driven magnon-magnon entanglement at room temperature, *New J. Phys.* **25**, 113032 (2023).
- [36] Y.-l. Ren, J.-k. Xie, X.-k. Li, S.-l. Ma, and F.-l. Li, Long-range generation of a magnon-magnon entangled state, *Phys. Rev. B* **105**, 094422 (2022).
- [37] Y.-P. Wang, J. W. Rao, Y. Yang, P.-C. Xu, Y. S. Gui, B. M. Yao, J. Q. You, and C.-M. Hu, Nonreciprocity and Unidirectional Invisibility in Cavity Magnonics, *Phys. Rev. Lett.* **123**, 127202 (2019).
- [38] J. Zhao, Y. Liu, L. Wu, C.-K. Duan, Y.-x. Liu, and J. Du, Observation of Anti- \mathcal{PT} -Symmetry Phase Transition in the Magnon-Cavity-Magnon Coupled System, *Phys. Rev. Appl.* **13**, 014053 (2020).
- [39] X.-L. Hei, X.-L. Dong, J.-Q. Chen, C.-P. Shen, Y.-F. Qiao, and P.-B. Li, Enhancing spin-photon coupling with a micromagnet, *Phys. Rev. A* **103**, 043706 (2021).
- [40] H. Y. Yuan, P. Yan, S. Zheng, Q. Y. He, K. Xia, and M.-H. Yung, Steady Bell State Generation via Magnon-Photon Coupling, *Phys. Rev. Lett.* **124**, 053602 (2020).
- [41] S.-f. Qi and J. Jing, Generation of Bell and Greenberger-Horne-Zeilinger states from a hybrid qubit-photon-magnon system, *Phys. Rev. A* **105**, 022624 (2022).
- [42] R. Hisatomi, A. Osada, Y. Tabuchi, T. Ishikawa, A. Noguchi, R. Yamazaki, K. Usami, and Y. Nakamura, Bidirectional conversion between microwave and light via ferromagnetic magnons, *Phys. Rev. B* **93**, 174427 (2016).
- [43] C. Zhao, X. Li, S. Chao, R. Peng, C. Li, and L. Zhou, Simultaneous blockade of a photon, phonon, and magnon induced by a two-level atom, *Phys. Rev. A* **101**, 063838 (2020).
- [44] Y. jun Xu, T. le Yang, L. Lin, and J. Song, Conventional and unconventional magnon blockades in a qubit-magnon hybrid quantum system, *J. Opt. Soc. Am. B* **38**, 876 (2021).
- [45] K. Wu, W.-x. Zhong, G.-l. Cheng, and A.-x. Chen, Phase-controlled multimagnon blockade and magnon-induced tunneling in a hybrid superconducting system, *Phys. Rev. A* **103**, 052411 (2021).
- [46] F. Wang, C. Gou, J. Xu, and C. Gong, Hybrid magnon-atom entanglement and magnon blockade via quantum interference, *Phys. Rev. A* **106**, 013705 (2022).
- [47] Z.-y. Jin and J. Jing, Magnon blockade in magnon-qubit systems, *Phys. Rev. A* **108**, 053702 (2023).
- [48] H. Y. Yuan and R. A. Duine, Magnon antibunching in a nanomagnet, *Phys. Rev. B* **102**, 100402 (2020).
- [49] Y.-T. Yan, C. Zhao, D.-W. Wang, J. Yang, and L. Zhou, Simultaneous blockade of two remote magnons induced by an atom, *Phys. Rev. A* **109**, 023710 (2024).
- [50] Z.-y. Jin and J. Jing, Stabilizing a single-magnon state by optimizing magnon blockade, *Phys. Rev. A* **110**, 012459 (2024).
- [51] D.-Y. Wang, C.-H. Bai, X. Han, S. Liu, S. Zhang, and H.-F. Wang, Enhanced photon blockade in an optomechanical system with parametric amplification, *Opt. Lett.* **45**, 2604 (2020).
- [52] C. J. Zhu, K. Hou, Y. P. Yang, and L. Deng, Hybrid level anharmonicity and interference-induced photon blockade in a two-qubit cavity QED system with dipole-dipole interaction, *Photon. Res.* **9**, 1264 (2021).
- [53] Z.-G. Lu, C. Shang, Y. Wu, and X.-Y. Lü, Analytical approach to higher-order correlation functions in U(1) symmetric systems, *Phys. Rev. A* **108**, 053703 (2023).
- [54] Z. Wu, J. Li, and Y. Wu, Phase-engineered photon correlations in weakly coupled nanofiber cavity QED, *Phys. Rev. A* **109**, 033709 (2024).
- [55] C. Couteau, S. Barz, T. Durt, T. Gerrits, J. Huwer, R. Prevedel, J. Rarity, A. Shields, and G. Weihs, Applications of single photons to quantum communication and computing, *Nat. Rev. Phys.* **5**, 326 (2023).
- [56] X. Wang, K.-W. Huang, and H. Xiong, Magnon blockade in a QED system with a giant spin ensemble and a giant atom coupled to a waveguide, *Phys. Rev. A* **110**, 033702 (2024).
- [57] S. He, X. Xin, F.-Y. Zhang, and C. Li, Generation of a Schrödinger cat state in a hybrid ferromagnet-superconductor system, *Phys. Rev. A* **107**, 023709 (2023).
- [58] X.-F. Pan, P.-B. Li, X.-L. Hei, X. Zhang, M. Mochizuki, F.-L. Li, and F. Nori, Magnon-Skyrmion Hybrid Quantum Sys-

- tems: Tailoring Interactions via Magnons, *Phys. Rev. Lett.* **132**, 193601 (2024).
- [59] Z. Li, M. Ma, Z. Chen, K. Xie, and F. Ma, Interaction between magnon and skyrmion: Toward quantum magnonics, *J. Appl. Phys.* **132**, 214401 (2022).
- [60] C. Reichhardt, C. J. O. Reichhardt, and M. V. Milošević, Statics and dynamics of skyrmions interacting with disorder and nanostructures, *Rev. Mod. Phys.* **94**, 035005 (2022).
- [61] K. Everschor-Sitte, J. Masell, R. M. Reeve, and M. Kläui, Perspective: Magnetic Skyrmions—Overview of Recent Progress in an Active Research Field, *J. Appl. Phys.* **124** (2018).
- [62] L. Liensberger, F. X. Haslbeck, A. Bauer, H. Berger, R. Gross, H. Huebl, C. Pfleiderer, and M. Weiler, Tunable cooperativity in coupled spin-cavity systems, *Phys. Rev. B* **104**, L100415 (2021).
- [63] T. Hirose, A. Mook, J. Klinovaja, and D. Loss, Magneto-electric Cavity Magnonics in Skyrmion Crystals, *Phys. Rev. X* **Quantum** **3**, 040321 (2022).
- [64] H. Ochoa and Y. Tserkovnyak, Quantum skyrmionics, *Int. J. Mod. Phys. B* **33**, 1930005 (2019).
- [65] C. Back, V. Cros, H. Ebert, K. Everschor-Sitte, A. Fert, M. Garst, T. Ma, S. Mankovsky, T. L. Monchesky, M. Mostovoy, N. Nagaosa, S. S. P. Parkin, C. Pfleiderer, N. Reyren, A. Rosch, Y. Taguchi, Y. Tokura, K. von Bergmann, and J. Zang, The 2020 skyrmionics roadmap, *J. Phys. D: Appl. Phys.* **53**, 363001 (2020).
- [66] C. Psaroudaki and C. Panagopoulos, Skyrmion Qubits: A New Class of Quantum Logic Elements Based on Nanoscale Magnetization, *Phys. Rev. Lett.* **127**, 067201 (2021).
- [67] P.-J. Hsu, A. Kubetzka, A. Finco, N. Romming, K. von Bergmann, and R. Wiesendanger, Electric-field-driven switching of individual magnetic skyrmions, *Nat. Nanotechnol.* **12**, 123 (2016).
- [68] M. T. Birch, I. Belopolski, Y. Fujishiro, M. Kawamura, A. Kikkawa, Y. Taguchi, M. Hirschberger, N. Nagaosa, and Y. Tokura, Dynamic transition and Galilean relativity of current-driven skyrmions, *Nature* **633**, 554 (2024).
- [69] M. Lonsky and A. Hoffmann, Dynamic Excitations of Chiral Magnetic Textures, *APL Materials* **8** (2020).
- [70] A. Bogdanov and A. Hubert, Thermodynamically stable magnetic vortex states in magnetic crystals, *J. Magn. Mater.* **138**, 255 (1994).
- [71] U. K. Röbber, A. N. Bogdanov, and C. Pfleiderer, Spontaneous skyrmion ground states in magnetic metals, *Nature* **442**, 797 (2006).
- [72] S. Mühlbauer, B. Binz, F. Jonietz, C. Pfleiderer, A. Rosch, A. Neubauer, R. Georgii, and P. Böni, Skyrmion Lattice in a Chiral Magnet, *Science* **323**, 915 (2009).
- [73] X. Z. Yu, Y. Onose, N. Kanazawa, J. H. Park, J. H. Han, Y. Matsui, N. Nagaosa, and Y. Tokura, Real-space observation of a two-dimensional skyrmion crystal, *Nature(London)* **465**, 901 (2010).
- [74] F. Jonietz, S. Mühlbauer, C. Pfleiderer, A. Neubauer, W. Münzer, A. Bauer, T. Adams, R. Georgii, P. Böni, R. A. Duine, K. Everschor, M. Garst, and A. Rosch, Spin Transfer Torques in MnSi at Ultralow Current Densities, *Science* **330**, 1648 (2010).
- [75] T. Schulz, R. Ritz, A. Bauer, M. Halder, M. Wagner, C. Franz, C. Pfleiderer, K. Everschor, M. Garst, and A. Rosch, Emergent electrodynamics of skyrmions in a chiral magnet, *Nat. Phys.* **8**, 301 (2012).
- [76] S. X. Huang and C. L. Chien, Extended Skyrmion Phase in Epitaxial FeGe(111) Thin Films, *Phys. Rev. Lett.* **108**, 267201 (2012).
- [77] N. Nagaosa and Y. Tokura, Topological Properties and Dynamics of Magnetic Skyrmions, *Nat. Nanotechnol.* **8** (2013).
- [78] A. Fert, V. Cros, and J. Sampaio, Skyrmions on the track, *Nat. Nanotechnol.* **8**, 152 (2013).
- [79] A. Fert, N. Reyren, and V. Cros, Magnetic Skyrmions: Advances in Physics and Potential Applications, *Nat. Rev. Mater.* **2** (2017).
- [80] S. Bhowal and N. A. Spaldin, Magnetoelectric Classification of Skyrmions, *Phys. Rev. Lett.* **128**, 227204 (2022).
- [81] T. Kurumaji, T. Nakajima, M. Hirschberger, A. Kikkawa, Y. Yamasaki, H. Sagayama, H. Nakao, Y. Taguchi, T. hisa Arima, and Y. Tokura, Skyrmion lattice with a giant topological Hall effect in a frustrated triangular-lattice magnet, *Science* **365**, 914 (2019).
- [82] A. O. Leonov and M. Mostovoy, Multiply Periodic States and Isolated Skyrmions in an Anisotropic Frustrated Magnet, *Nat. Commun.* **6** (2015).
- [83] S.-Z. Lin and S. Hayami, Ginzburg-Landau theory for skyrmions in inversion-symmetric magnets with competing interactions, *Phys. Rev. B* **93**, 064430 (2016).
- [84] X. Zhang, J. Xia, Y. Zhou, X. Liu, H. Zhang, and M. Ezawa, Skyrmion dynamics in a frustrated ferromagnetic film and current-induced helicity locking-unlocking transition, *Nat. Commun.* **8**, 1717 (2017).
- [85] X. Yao, J. Chen, and S. Dong, Controlling the helicity of magnetic skyrmions by electrical field in frustrated magnets, *New J. Phys.* **22**, 083032 (2020).
- [86] J. Xia, X. Zhang, X. Liu, Y. Zhou, and M. Ezawa, Universal Quantum Computation Based on Nanoscale Skyrmion Helicity Qubits in Frustrated Magnets, *Phys. Rev. Lett.* **130**, 106701 (2023).
- [87] P. Rabl, Photon Blockade Effect in Optomechanical Systems, *Phys. Rev. Lett.* **107**, 063601 (2011).
- [88] Y.-x. Liu, A. Miranowicz, Y. B. Gao, J. c. v. Bajer, C. P. Sun, and F. Nori, Qubit-induced phonon blockade as a signature of quantum behavior in nanomechanical resonators, *Phys. Rev. A* **82**, 032101 (2010).
- [89] L.-L. Zheng, T.-S. Yin, Q. Bin, X.-Y. Lü, and Y. Wu, Single-photon-induced phonon blockade in a hybrid spin-optomechanical system, *Phys. Rev. A* **99**, 013804 (2019).
- [90] Y.-W. Lu, J.-F. Liu, R. Li, Y. Wu, H. Tan, and Y. Li, Single-photon blockade in quasichiral atom-photon interaction: simultaneous high purity and high efficiency, *New J. Phys.* **24**, 053029 (2022).
- [91] H. Flayac and V. Savona, Unconventional photon blockade, *Phys. Rev. A* **96**, 053810 (2017).
- [92] H. Xie, C.-G. Liao, X. Shang, M.-Y. Ye, and X.-M. Lin, Phonon blockade in a quadratically coupled optomechanical system, *Phys. Rev. A* **96**, 013861 (2017).
- [93] X.-W. Xu, A.-X. Chen, and Y.-x. Liu, Phonon blockade in a nanomechanical resonator resonantly coupled to a qubit, *Phys. Rev. A* **94**, 063853 (2016).
- [94] H. Carmichael, *Statistical Methods in Quantum Optics* (Springer, Berlin, 1999).
- [95] D. Ghazaryan, M. T. Greenaway, Z. Wang, V. H. Guarochico-Moreira, I. J. Vera-Marun, J. Yin, Y. Liao, S. V. Morozov, O. Kristanovski, A. I. Lichtenstein, M. I. Katsnelson, F. Withers, A. Mishchenko, L. Eaves, A. K. Geim, K. S. Novoselov, and A. Misra, Magnon-assisted tunnelling in van der Waals heterostructures based on CrBr₃, *Nat. Electron.* **1**, 344 (2018).
- [96] C. Gonzalez-Ballester, D. Hümmer, J. Gieseler, and O. Romero-Isart, Theory of quantum acoustomagnonics and acoustomechanics with a micromagnet, *Phys. Rev. B* **101**, 125404 (2020).

- [97] C. Gonzalez-Ballester, J. Gieseler, and O. Romero-Isart, Quantum Acoustomechanics with a Micromagnet, *Phys. Rev. Lett.* **124**, 093602 (2020).
- [98] C. Psaroudaki, E. Peraticos, and C. Panagopoulos, Skyrmion qubits: Challenges for future quantum computing applications, *Appl. Phys. Lett.* **123**, 26 (2023).
- [99] X.-F. Pan, X.-L. Hei, X.-Y. Yao, J.-Q. Chen, Y.-M. Ren, X.-L. Dong, Y.-F. Qiao, and P.-B. Li, Skyrmion-mechanical hybrid quantum systems: Manipulation of skyrmion qubits via phonons, *Phys. Rev. Res.* **6**, 023067 (2024).
- [100] S. Fujita, A. Suzuki, and H.-C. Ho, Composite-Particles (Boson, Fermion) Theory of Fractional Quantum Hall Effect, *Int. J. Theor. Phys.* **56**, 396 (2016).
- [101] P. Kómár, S. D. Bennett, K. Stannigel, S. J. M. Habraken, P. Rabl, P. Zoller, and M. D. Lukin, Single-photon nonlinearities in two-mode optomechanics, *Phys. Rev. A* **87**, 013839 (2013).
- [102] J. Tang, Y. Deng, and C. Lee, Strong Photon Blockade Mediated by Optical Stark Shift in a Single-Atom-Cavity System, *Phys. Rev. Appl.* **12**, 044065 (2019).
- [103] M. O. Scully and M. S. Zubairy, *Quantum Optics* (Cambridge University Press, Cambridge, 1997).
- [104] J. R. Johansson, P. D. Nation, and F. Nori, QuTiP 2: A Python framework for the dynamics of open quantum systems, *Comput. Phys. Commun.* **184**, 1234 (2013).
- [105] Y. Tabuchi, S. Ishino, A. Noguchi, T. Ishikawa, R. Yamazaki, K. Usami, and Y. Nakamura, Coherent coupling between a ferromagnetic magnon and a superconducting qubit, *Science* **349**, 405 (2015).
- [106] J. T. Hou and L. Liu, Strong Coupling between Microwave Photons and Nanomagnet Magnons, *Phys. Rev. Lett.* **123**, 107702 (2019).